Modeling Manganese Sorption and Surface Oxidation During Filtration

Kevin Andrew Bierlein

Thesis submitted to the faculty of the Virginia Polytechnic Institute and State University in partial fulfillment of the requirements for the degree of

Master of Science

In

Environmental Engineering

John C. Little
William R. Knocke
John E. Tobiason

30 April 2012
Blacksburg, VA

Keywords: manganese, filtration, oxidation, sorption

Modeling Manganese Sorption and Surface Oxidation During Filtration

Kevin Andrew Bierlein

Abstract

Soluble manganese (Mn) is a common contaminant in drinking water sources. High levels of Mn can lead to aesthetic water quality problems, necessitating removal of Mn during treatment to minimize consumer complaints. Mn may be removed during granular media filtration by the "natural greensand effect," in which soluble Mn adsorbs to manganese oxide-coated ($MnO_x(s)$) media and is then oxidized by chlorine, forming more manganese oxide. This research builds on a previous model developed by Merkle et al. (1997) by either neglecting the empirically determined available fraction of sorption sites (referred to as the "simple" model), which took into account the fact that some adsorption sites in the porous media were inaccessible, or by explicitly accounting for the transport and reaction processes within the porous structure of the $MnO_x(s)$ coating (referred to as the "mechanistic" model). Both models were applied to experimental data and used to evaluate the oxidation rate constant, which was the only unknown parameter. An inverse relationship between the fitted reaction rate constant and chlorine concentration was observed, showing that the oxidation reaction does not depend on chlorine concentration for the experimental conditions considered. In a sensitivity analysis, the adsorption isotherm and reaction rate were found to have the greatest impact on predicted Mn removal. The simple model should prove useful for designing contactor units for manganese removal, provided its limitations are clearly understood, while the mechanistic model should be able to resolve differences in the various types of oxide coating (internal porosity, surface area and coating thickness) and will allow a more fundamental and mechanistically-consistent evaluation of the appropriate form of the oxidation rate expression. However, further research is needed to more completely characterize the adsorption and reaction mechanisms over the range of conditions commonly encountered in water treatment plants.

Acknowledgements

I am extremely grateful for the guidance, support, and encouragement from my advisor, Dr. John Little, while working towards this degree. I would also like to thank my committee members, Dr. William Knocke and Dr. John Tobiason for their valuable advice and input during the course of this research.

I would also like to express my sincere appreciation to Dr. Michael Williams, Dr. Daniel Gallagher, and Dr. Zhe Liu for their assistance and willingness to provide valuable comments and suggestions during the model development.

Finally, I would like to thank my family and friends for their unwavering support and encouragement in all that I do.

Table of Contents

List of Figures

List of Tables

Attributions

Several colleagues contributed to the research presented in this thesis, and a brief description of their backgrounds and contributions are included here. Mr. Kevin Bierlein (masters student, Department of Civil and Environmental Engineering, Virginia Tech) performed the primary research work and writing under the guidance of Dr. John C. Little (Professor, Department of Civil and Environmental Engineering, Virginia Tech; Advisor and Committee Chair) and their specific contributions will not be discussed in detail. Dr. William R. Knocke (Associate Vice President for Research Programs, Virginia Tech; Professor, Department of Civil and Environmental Engineering, Virginia Tech; Committee member) helped develop the research intellectually and provided the pilot-scale contactor column and adsorption isotherm experimental data. Dr. John E. Tobiason (Professor, Department of Civil and Environmental Engineering, University of Massachusetts Amherst; Committee member) helped develop the research intellectually. This manuscript is being prepared for submission to *Water Research*.

1.0 Introduction and Objectives

Manganese (Mn) is a naturally occurring metal found in many drinking water sources. It is frequently present in groundwater as well as in lakes and reservoirs, particularly during periods of thermal stratification (Bryant et al., 2011; Homoncik et al., 2010; Buamah et al., 2009; Gantzer et al., 2009). High levels of soluble manganese can cause aesthetic water quality problems, such as metallic taste, discolored water and a black staining of plumbing fixtures. To minimize consumer complaints, the U.S. Environmental Protection Agency secondary maximum contaminant level (SMCL) is set at 0.05 mg/L, although even lower manganese treatment targets in the range of 0.01 – 0.02 mg/L have been recommended (Knocke et al., 2010; Kohl and Medlar, 2006; Sly et al., 1990). Removal of soluble manganese is commonly achieved through oxidation by potassium permanganate, chlorine dioxide, ozone, or other strong oxidant (Kohl and Medlar, 2006; Gregory & Carlson, 2003). Removal is also possible using microbial oxidation under aerobic conditions (Mouchet, 1992) or sorption and oxidation of soluble manganese on media coated with manganese oxide ($MnO_x(s)$), also known as the "natural greensand effect" (Knocke et al., 2010).

Removal of Mn with an oxidant can be troublesome for a water utility. Careful dosing of potassium permanganate is required to avoid "pink water" events and high amounts of dissolved organic carbon (DOC) present during chlorination can result in elevated levels of disinfection byproducts (DBPs) (Hua & Reckhow, 2007). Some water utilities have ceased chlorine addition prior to their dual- or tri-media filters in an effort to comply with DBP standards, only to find that they no longer achieve Mn removal during filtration (Knocke et al., 2010). A possible solution for effective soluble Mn removal is the addition of a contactor unit that is designed to take advantage of the natural greensand effect. Such a filter can be sized to minimize head loss while reliably and effectively removing Mn. For design purposes, a sound knowledge of Mn transport and transformation processes within the contactor, including the mechanisms of adsorption and surface oxidation, is required.

1.1 Previous Modeling Efforts

The removal of manganese by sorption and surface oxidation during filtration can be described by the following equations (Coffey et al., 1993; Nakanishi 1967):

$$Mn^{2+} + MnO(OH)_{2(s)} \underset{k_2}{\overset{k_1}{\rightleftharpoons}} MnO_2MnO_{(s)} + 2H^+ \quad (1)$$

$$MnO_2MnO_{(s)} + HOCl \underset{k_2}{\overset{k_1}{\rightleftharpoons}} 2MnO_{2(s)} + H^+ + Cl^- \quad (2)$$

Soluble Mn adsorbs to MnO_x(s)-coated media and is subsequently oxidized by HOCl, forming additional MnO_x(s). This is, in essence, a self-regenerating process in which the MnO_x(s) acts as a catalyst for Mn^{2+} removal via oxidation by HOCl. Recent research by Cerrato et al. (2011) showed that in the presence of sufficient chlorine, Mn^{2+} adsorbed to MnO_x(s)-coated media is quickly oxidized to Mn(IV), which does not readily dissolve back into the water. Research to describe and model the removal of manganese during granular media filtration based on equations 1 and 2 has been undertaken by Nakanishi (1967), Coffey et al. (1993) and Merkle et al. (1997). Nakanishi's model was published in Japanese and unfortunately never translated into English. Coffey modeled the manganese removal under both continuous (steady-state) and intermittent regeneration conditions (where regeneration refers to the presence of an oxidant which "regenerates" the oxide surface), finding the model to potentially be a useful tool in designing filters for manganese removal. Coffey noted, however, that a better understanding of the Mn^{2+} adsorption process may be required for developing a more reliable model. Merkle also modeled the adsorption and oxidation process under continuous and intermittent regeneration conditions, although the model was based on equation 3, which is a simplified version of equations 1 and 2.

$$Mn^{2+} + SITE + HOCl \rightarrow MnO_{x(s)} + SITE \quad (3)$$

Merkle's model predicted mass transfer from the bulk water to the exterior media surface, and represented adsorption to the media with a Freundlich isotherm. The model incorporated an empirical parameter referred to as the "AFR", or available fraction of sorption sites, that took into account the fact that some adsorption sites in the porous media were inaccessible. The AFR was identified by calibrating the model to experimental data. It was also noted that the presence of additional species in the water, such as dissolved organic carbon (DOC) or calcium, might negatively affect the performance of the filter by exerting an additional chlorine demand or by interfering with adsorption to the MnO_x(s) coating.

This research builds on Merkle's model by either neglecting the AFR in a simplified version of the model (referred to as the simple model) or by taking diffusion into the porous media into account in a mechanistic fashion (referred to as the mechanistic model). The mechanistic model

accounts for the diffusive flux of Mn and chlorine into the pore water within the porous media grains, as well as the subsequent adsorption and oxidation that takes place on the interior pore surfaces.

1.2 Research Objectives

The main objective of this study was to develop an improved model of sorption and surface oxidation of manganese during filtration. Both the simple model (which was previously developed by Zuravnsky (2006) and used by Subramaniam (2010) and Pham (2010)) and the new mechanistic model were applied to previously collected experimental data with results used to evaluate the validity of the assumed oxidation rate expression and the rate constant. Additional objectives were to perform a simple sensitivity analysis to identify the controlling mechanisms in the filtration process, and to evaluate the utility of the simple and mechanistic models.

2.0 Model Development

2.1 Simple Model Development

Graphical representations of a media contactor column and an incremental volume of filter media are shown in Figures 1 and 2. The simple model simulates the manganese removal process with advection and dispersion within the contactor column, followed by mass transfer through the boundary layer surrounding the media grains, and then adsorption and surface oxidation. Equations 4 through 7 are the mass balance equations describing manganese and chlorine transport processes. The mass-transfer coefficient (k_f), Sherwood number (Sh), and axial dispersion coefficient (D_L) are calculated according to Roberts et al. (1985) and Delgado (2007), using equations 8 through 10, respectively. Further details of the model derivation are provided in Appendix A.

$$\frac{\partial C_{1B}}{\partial t} = 0 = -U\frac{\partial C_{1B}}{\partial z} + D_L\frac{\partial^2 C_{1B}}{\partial z^2} - k_f A_{V,M}\left(\frac{1-\varepsilon_B}{\varepsilon_B}\right)\left(C_{1B} - \left[\frac{C_{1sa}}{K_s}\right]^n\right) \tag{4}$$

$$\frac{\partial C_{2B}}{\partial t} = 0 = -U\frac{\partial C_{2B}}{\partial z} + D_L\frac{\partial^2 C_{2B}}{\partial z^2} - \rho_B k_r C_{1sa} C_{2B} \tag{5}$$

$$\frac{\partial C_{1sa}}{\partial t} = 0 = \frac{k_f A_{V,M}}{\rho_B}\left(1-\varepsilon_B\right)\left[C_{1B} - \left[\frac{C_{1sa}}{K_s}\right]^n\right] - k_r \varepsilon_B C_{1sa} C_{2B} \tag{6}$$

$$C_{1B,in} - C_{1B,out} = C_{2B,in} - C_{2B,out} \tag{7}$$

where: $A_{V,M}$ = Specific external surface area of media ($m^2_{media}\ m^{-3}_{media}$)

C_{1B} = Bulk aqueous-phase Mn concentration (mol m^{-3})

C_{1sa} = Adsorbed-phase Mn concentration (mol kg^{-1})

C_{2B} = Bulk aqueous-phase HOCl concentration (mol m^{-3})

D_L = Axial dispersion coefficient ($m^2\ s^{-1}$)

ε_B = Fractional column pore volume ($m^3_{water}\ m^{-3}_{bed}$)

K_s = Freundlich isotherm constant ([mol kg^{-1}] [mol m^{-3}]$^{-n}$)

k_f = Mass-transfer coefficient (m s^{-1})

k_r = Oxidation rate constant ($m^3_{bed}\ mol^{-1}\ s^{-1}$)

n = Freundlich isotherm constant (dimensionless)

ρ_B = Media bulk density ($kg_{media}\ m^{-3}_{bed}$)

U = Average column pore water velocity (m s^{-1})

z = Depth in media bed (m)

$$k_f = \frac{Sh \cdot D_m}{dp} \tag{8}$$

where: dp = Mean media particle diameter (m)

Sh = Sherwood number (dimensionless)

$$Sh = \left[2 + 1.21 \mathrm{Re}^{0.5} Sc^{1/3}\right] \tag{9}$$

where: D_m = Molecular diffusivity ($m^2\ s^{-1}$)

Re = Reynolds number (dimensionless) = $\frac{U \cdot dp}{\mu}$

Sc = Schmidt number (dimensionless) = $\frac{\mu}{D_m}$

μ = Kinematic viscocity ($m^2\ s^{-1}$)

$$\frac{D_L}{D'_m} = \frac{Pe'_m}{\left(25 \cdot Sc^{1.14} \Big/ Pe'_m + 0.5\right)} \tag{10}$$

where: D'_m = Effective molecular diffusivity ($m^2\ s^{-1}$) = $\frac{D_m}{\tau}$

Pe'_m = Effective Peclet number of inert particle (dimensionless) = $\frac{U \cdot dp}{D'_m}$

τ = Tortuosity factor (dimensionless)

This model is a simplification of Merkle's model in that it ignores the AFR, with adsorption and surface oxidation assumed to occur on the external surface of the media grains. The simple model assumes steady state conditions with continuous regeneration by chlorine. It is also assumed that no additional species are present that might interfere with adsorption or oxidation, and that there is no increase in media grain diameter or adsorption capacity due to deposited $MnO_x(s)$. Because chlorine is usually present in excess, it is further assumed that the concentration of chlorine in the boundary layer surrounding the granular media is equal to the chlorine concentration in the bulk water, rather than explicitly accounting for mass transfer of chlorine to the media surface. Thus, in the terms that account for the removal of Mn via oxidation on the right-hand side of equations 5 and 6, the chlorine concentration is given by C_{2B}, which is the concentration in the bulk water. If the experimental conditions were such that chlorine was not present in excess, mass transfer of chlorine from the bulk water to the media surface would need to be taken into account.

With the exception of the oxidation rate constant (k_r) all parameters were calculated as described above or determined from experimental measurements as described in Section 3. The oxidation rate constant was the only unknown parameter and was determined by fitting the model output to experimental data. Best-fit values for k_r were determined using a Levenberg-Marquardt non-linear regression algorithm. The model was coded using the open-source statistics program R.

2.2 Mechanistic Model Development

Figure 3 provides a graphical representation of the bulk water and media pore water mass balances for the mechanistic model. The mechanistic approach accounts for diffusion of Mn and chlorine into the media pore water and the subsequent adsorption and surface oxidation reaction that takes place within the pores, using coupled equations that separately account for transport processes in the contactor column and in the porous media grains. Equations 11 and 12 describe the mass balance in the bulk water, accounting for transport due to advection and mass transfer through the boundary layer. Equations 13 and 14 describe a mass balance in the pore water within a porous media grain, accounting for diffusion within the pore water, adsorption to the internal media grain surface, and the subsequent chemical reaction. This eliminates the need for the empirical AFR parameter.

$$\frac{\partial C_{1B}}{\partial t} = 0 = -U\frac{\partial C_{1B}}{\partial z} - k_f A_{V,M}\left(\frac{1-\varepsilon_B}{\varepsilon_B}\right)\left(C_{1B} - C_{1sa}\right) \tag{11}$$

$$\frac{\partial C_{2B}}{\partial t} = 0 = -U\frac{\partial C_{2B}}{\partial z} - k_f A_{V,M}\left(\frac{1-\varepsilon_B}{\varepsilon_B}\right)\left(C_{2B} - C_{2sa}\right) \tag{12}$$

$$\frac{\partial C_1}{\partial t} = 0 = -\frac{D_1}{\varepsilon_A}\frac{\partial^2 C_1}{\partial x^2} - k_r A_{V,A} K_m C_1^n C_2 \tag{13}$$

$$\frac{\partial C_2}{\partial t} = 0 = -\frac{D_2}{\varepsilon_A}\frac{\partial^2 C_2}{\partial x^2} - k_r A_{V,A} K_m C_1^n C_2 \tag{14}$$

$$k_f\left(C_{1B} - C_{1sa}\right) = J_1 = -D_1\frac{dC_1}{dx} \tag{15}$$

$$k_f\left(C_{2B} - C_{2sa}\right) = J_2 = -D_2\frac{dC_2}{dx} \tag{16}$$

where: $A_{V,A}$ = Specific internal surface area of media grain ($m^2_{\text{active grain}}$ $m^{-3}_{\text{active grain}}$)

C_1 = Manganese concentration in the media pore water (mol m^{-3}_{water})

C_{1sa} = Manganese concentration at media grain surface (mol m^{-3}_{water})

C_2 = Chlorine concentration in the media pore water (mol m^{-3}_{water})

C_{2sa} = Chlorine concentration at media grain surface (mol m^{-3}_{water})
D_1 = Manganese diffusion coefficient (m^3_{water} $m^{-1}_{active\ grain}$ s^{-1})
D_2 = Chlorine diffusion coefficient (m^3_{water} $m^{-1}_{active\ grain}$ s^{-1})
ε_A= Porosity of active grain (m^3_{water} $m^{-3}_{active\ grain}$)
x = Distance into media grain ($m_{active\ grain}$)
K_m = Freundlich isotherm constant ([mol $m^{-2}_{active\ grain}$] [mol m^{-3}_{water}]$^{-n}$)
J_1 = Manganese flux into media grain pore water (mol $m^{-2}_{active\ grain}$ s^{-1})
J_2 = Chlorine flux into media grain pore water (mol $m^{-2}_{active\ grain}$ s^{-1})

This mechanistic approach explicitly accounts for mass transfer of chlorine from the bulk water through the boundary layer, rather than assuming that the boundary layer concentration is equal to the bulk water concentration. Thus, in the oxidation terms on the right-hand side of equations 13 and 14, the chlorine concentration is given by C_2, which is the concentration in the media pore water. It is also assumed that dispersion in the bulk water is negligible, that the reaction takes place entirely within the media pore, and that surface diffusion of adsorbed Mn is negligible because oxidation is rapid. Also, Mn adsorption to the MnO_x(s) takes place via chemical adsorption, rather than physical adsorption, and this may also reduce the potential for surface diffusion. Because the reaction is rapid relative to diffusion, it is assumed that transport within the media pores occurs only in a relatively thin outer portion of the MnO_x(s) coating. This means that spherical coordinates are not necessary and that diffusion and reaction within the porous media can be assumed to occur in a flat or planar region. The bulk water portion of the model is coupled to the media pore water portion by setting mass transfer from the bulk water to the media surface equal to the diffusive flux into the media pore water. Equations 15 and 16 show this relationship for Mn and chlorine, respectively.

The major difference between the simple and mechanistic model is that the mechanistic model considers diffusion and reaction of manganese and chlorine as they penetrate into the porous media coating, rather than assuming that adsorption and oxidation occurs only on the exterior media surface. Dispersion in the bulk water is neglected because it was shown to be inconsequential using the simple model. As with the simple model, all parameters were calculated or measured experimentally except the oxidation rate constant, which was obtained by fitting the model to experimental data. Diffusion coefficients for Mn ($D_1 = 6.88\times10^{-10}$ m^2 s^{-1}) and HOCl ($D_2 = 1.90\times10^{-9}$ m^2 s^{-1}) were obtained from Domenico & Schwartz (1998) and Davison et al., (2010), respectively. The mechanistic model was coded using Matlab. The media pore water portion was solved using the bvp4c solver function, and the bulk water portion was solved using Euler's method. Since Matlab lacks a built-in Levenberg-Marquardt nonlinear

regression algorithm, a least-squares approach was used to determine the best-fit value for k_r. Further details of the model derivation are provided in Appendix B.

3.0 Experimental Measurements

3.1 Column Experiments

The data sets used to evaluate the oxidation rate constant were obtained from a pilot-scale study performed by Subramaniam (2010) using a proprietary $MnO_x(s)$ media, pyrolucite. The influent water had Mn concentrations ranging from 1.0×10^{-3} to 1.8×10^{-3} mol m^{-3} (0.06 to 0.1 mg L^{-1}), pH 6.5 to 7.5, temperature of 20°C (68°F), hydraulic loading rates (HLR) ranging from 0.65 to 0.98 m^3 min^{-1} m^{-2} (16 to 24 gallons min^{-1} ft^{-2}), and total chlorine concentrations varying from 1.5×10^{-2} to 7.3×10^{-2} mol m^{-3} (0.5 to 5 mg L^{-1}). The bed porosity (ε_B) of the contactor column was 0.52 and the pyrolucite media had an average particle size of 2.2 mm, bulk density (ρ_B) of 1992 kg_{media} $m^{-3}{}_{bed}$ and specific external surface area ($A_{V,M}$) of 7260 $m^2{}_{media}$ $m^{-3}{}_{media}$. A detailed description of the pilot-scale study is provided by Subramaniam (2010).

3.2 Isotherm Experiments

The Freundlich isotherm constants (K_s, n) used to represent the sorption of soluble Mn to the oxide-coated media were determined in experiments performed by Subramaniam using a recycle method developed by Tobiason et al., (2008). A reservoir of water with a known soluble Mn concentration is circulated through a media column for four hours, after which the final concentration of soluble Mn is measured. The uptake capacity (q) is calculated as shown in equation 17. Values for the Freundlich isotherm constants can then be found by plotting $\ln(q)$ versus $\ln(C_f)$. The equation for a linear trend line fitted to this plot is analogous to the linearized form of the Freundlich isotherm equation (equation 18), which allows the values of K_s and n to be determined.

$$q = \frac{V\left(C_i - C_f\right)}{M} \tag{17}$$

$$\ln\left(q\right) = \ln\left(K_s\right) + n\ln\left(C_f\right) \tag{18}$$

where: C_i = Initial soluble Mn concentration (mg L^{-1})

C_f = Final soluble Mn concentration (mg L^{-1})

M = Mass of media in column (g)

q = Mn uptake capacity of media (mg Mn g^{-1})

V = Volume of solution in reservoir (L)

3.3 Porosity Experiment

The internal porosity of the pyrolucite media grains themselves was measured experimentally. Samples of media were saturated with nanopure water to fill the internal media pore volume.

Excess water between media grains was allowed to drain and the saturated media was weighed, dried overnight at 105°C, and weighed again. The porosity was calculated by dividing the volume of water evaporated by the volume of the dried media, with the assumption that the pyrolucite media has a porous structure throughout, as opposed to a MnO_x(s)-coated media, which would have a porous coating and solid internal structure.

4.0 Results and Discussion

4.1 Experimental Measurement Results

A detailed explanation of the pilot-scale contactor column results may be found in Submanraniam (2010). The pyrolucite contactor column Mn profiles from that study were used as the experimental data sets for fitting the models. The values of the Freundlich isotherm constants (K_s, n) obtained for a water temperature of 20°C were K_s=0.72 [mol kg^{-1}] [mol m^{-3}]$^{-n}$ and n=0.83 at pH 6.5 and K_s=0.88 [mol kg^{-1}] [mol m^{-3}]$^{-n}$ and n=0.84 at pH 7.5. Values for K_m used in the mechanistic model were calculated based on K_s by a simple unit conversion. The calculated internal porosity of the pyrolucite media was 0.47. Using this internal porosity value, as well as a BET isotherm obtained by Tobiason et al. (2008), the specific internal surface area of the pyrolucite media ($A_{V,A}$) was estimated as 1.2×10^8 m^2 m^{-3}. For comparison, this equates to 29 m^2 g^{-1} which is much lower than values typical of granular activated carbon, which are on the order of 10^2 - 10^3 m^2 g^{-1} (Bansal & Goyal, 2005).

4.2 Evaluation of Oxidation Rate Expression and Rate Constant

Both the simple and mechanistic models were fitted to each of the eight data sets from the pilot-scale study (runs A1 through A8) with the temperature-dependent model constants (D_1, D_2, D_L, D_m, μ) evaluated for a water temperature of 20°C. The fitted k_r values are shown in Table 1. The initial fitting of the models took into account the pH effect on speciation of total chlorine into HOCl and OCl^-, assuming that only the HOCl fraction reacts with the adsorbed Mn because HOCl is a strong oxidant. At pH 6.5, HOCl makes up approximately 90% of the total chlorine, while at pH 7.5, the HOCl fraction is only about 45% of the total chlorine. Because OCl^- may act as a weak oxidant, and because it equilibrates rapidly with HOCl, both models were again applied to the experimental data, this time assuming that the oxidant concentration is equal to HOCl + OCl^-. Thus, two sets of fitted k_r values are derived for both the simple and mechanistic models, as shown in Table 1. For the HOCl-only condition, fitted values of k_r ranged from 5.6×10^{-3} to 4.5×10^{-2} m^3 mol^{-1} s^{-1} in the simple model and from 1.5×10^{-3} to 1.8×10^{-2} m^3 mol^{-1} s^{-1} in the mechanistic model. Fitted k_r values for the HOCl + OCl^- condition ranged from 7.0×10^{-3} to 3.3×10^{-2} m^3 mol^{-1} s^{-1} in the simple model and from 1.5×10^{-3} to 9.2×10^{-3} m^3 mol^{-1} s^{-1} in the mechanistic model. Generally speaking, fitted k_r values with the simple model under the HOCl + OCl^- condition were lower at pH 7.5 and higher at pH 6.5, when compared to the same data set fitted under the HOCl-only condition, however this pattern did not hold for the values fitted with the mechanistic model.

The k_r values from the mechanistic model are consistently lower than the values from the simple model. A possible reason for this observed difference is the increased surface area of the mechanistic model. Since there are more sites available for Mn to adsorb to, the reaction rate required to remove an equivalent amount of Mn from the bulk water is lower. Another possibility is that diffusion into the media pores is accounted for in the mechanistic model, but would be lumped into the fitted value of k_r in the simple model.

Both models fit the experimental data well, as shown in Figure 4, which includes a Mn profile from the simple and mechanistic models, each compared to the same experimental data set. Additionally, Figures 5 and 6 show predicted media pore water manganese and chlorine profiles generated with the mechanistic model at depths of 0, 35, and 70 cm (top, middle and bottom) in the contactor column. Although there is no comparable in-pore experimental data, the results make conceptual sense. With increased distance into the media grain, Mn and chlorine decrease as they react with one another until the limiting reactant (adsorbed Mn in this case) is depleted. With increasing depth in the contactor column, and consequently decreased bulk water Mn and chlorine concentrations, the initial concentrations at the entrance to the media pores are also lower. In all three profiles shown in Figure 5, essentially all the Mn has been removed from the media pore water within the first 0.2 mm. Since the nominal media grain radius is 1.1 mm, this means that all of the adsorption and oxidation of Mn occurs in the outer 18% of the media grain, justifying the assumption of planar coordinates. Pyrolucite media is porous throughout, however other MnO_x(s)-coated media typically have coatings approximately 0.1 mm thick, and may be as thick as 0.2 mm (Tobiason et al., 2008). Therefore, the media pore water profiles for a coated media may be different to those obtained here for pyrolucite, with the manganese only penetrating to a depth in the media equal to the thickness of the MnO_x(s) coating.

Interestingly, the fitted k_r values are found to be inversely proportional to the chlorine concentration, as shown in Figure 7. In fact, the inverse relationship is created because the rate of the reaction is assumed to be proportional to both chlorine and adsorbed Mn concentrations. This dependence is shown in equations 5 and 6 for the simple model, and equations 13 and 14 for the mechanistic model. When the rate constant is fitted to the data, the inherent lack of dependence on the chlorine concentration forces an almost perfect inverse relationship between the resulting k_r and the chlorine concentration. To confirm this observation, the reaction term in equations 5 and 6 was rewritten as a simple first-order reaction, dependent only on the concentration of adsorbed Mn, and eliminating the dependence on the chlorine concentration (C_{2B}). When the simple model was again applied to the experimental data, the resulting first-order rate constant ($k_{r,1}$) values range from 2.8×10^{-4} to 5.2×10^{-4} s^{-1}, as shown in Table 1. The

results no longer show an inverse relationship between $k_{r,1}$ and the chlorine concentration, and the coefficient of variation (standard deviation divided by the mean) of 0.22 is much lower than for the second-order rate constants (with coefficients of variation that range from 0.46 to 0.78). The fitted first-order rate constant values are similar to those determined by Pham (2010), which ranged from 0.8×10^{-4} to 1.8×10^{-4} s^{-1}. Differences between the first-order fitted rate constants from this study and those determined by Pham (2010) are likely a result of differences in source water quality, such as organic matter or other metals, which are not accounted for in the model. This shows that for the conditions used when generating this specific set of experimental data, with chlorine in substantial excess compared to Mn, the rate of the reaction is actually independent of the chlorine concentration and dependent only on the adsorbed Mn concentration. Presumably the reaction would depend on chlorine at a lower concentration, but further research is required to more completely characterize the reaction mechanism. Because of the similar behavior observed in the two models, the first-order fitting procedure was not repeated for the mechanistic model with the chlorine dependence removed.

4.3 Sensitivity Analysis

Using the simple model and operating conditions from data set A6, a sensitivity analysis was performed by adjusting parameters by ±50% to gain an insight into the dominant processes and important model parameters. For this analysis, the Freundlich isotherm constants (K_s, n), axial dispersion coefficient (D_L), mass transfer coefficient (k_f), and oxidation rate constant (k_r) were each varied in turn.

The results of the sensitivity analysis are displayed as predicted bulk water Mn profiles in Figures 8 through 12. Adsorption of Mn onto the media surface plays a vital role, as can be seen in Figures 8 and 9. The system is extremely sensitive to the Freundlich n parameter as evidenced by the noticeable change in shape of the predicted profiles. Interestingly, when adjusting K_s and k_r, the model behaves in a very similar manner (Figures 8 and 10). In fact, the profiles predicted by adjusting K_s by ±50% are identical to those predicted by adjusting k_r by ±50%. This behavior is observed in both models, but is easiest to understand mathematically by considering the media pore water Mn mass balance for the mechanistic model (equation 13). Considering the reaction term in this equation, it is clear that adjusting either K_m or k_r by the same amount will have the exact same effect. This relationship is not immediately obvious in the mass balance used for the simple model (equation 6), but it nevertheless exists, albeit in an alternative mathematical form. Overall, this behavior suggests that as the adsorptive capacity increases the oxidation rate will become limiting, and as the oxidation rate increases, adsorption will become limiting. Variation

in the mass transfer coefficient has less of an impact on the system than adsorption and oxidation. As the mass transfer rate decreases, it hinders Mn removal by slowing transport of Mn from the bulk solution to the media grain surface where it can be adsorbed and oxidized. When the mass transfer rate increases, Mn removal increases, but not to the extent caused by equivalent changes in the isotherm or oxidation rate. The system is least sensitive to axial dispersion, as shown in Figure 12. This is reasonable considering the relatively high hydraulic loading rates, and justifies the assumption made in the mechanistic model that axial dispersion is negligible.

4.4 Evaluation of Models

Although the simple and mechanistic models fit the experimental data equally well, the mechanistic model allows a clearer understanding by explicitly accounting for the internal porosity and surface area of the porous media grains, rather than having to empirically estimate these effects using the AFR parameter (Merkle et al., 1997). In the case of the pyrolucite media, the media grains are considered to be porous throughout, but for the more usual MnO_x(s)-coated sand grains, the thickness of the porous coating on the media would also be explicitly considered. When evaluating different types of media coating, the mechanistic model should be able to account for their different internal structures. If the oxidation rate expression needs to include the chlorine concentration, as it will likely do at lower chlorine concentrations than considered here, the mechanistic model takes into account the depletion of chlorine that occurs as a function of distance into the grain. For these reasons, the mechanistic model should enable a more comprehensive evaluation of the appropriate form of the oxidation rate expression, allowing the rate constants that are obtained to be more universally applicable.

There is a need for further work to more completely characterize the reaction mechanism over a wider range of conditions. Studies at lower chlorine concentrations should prove beneficial as they may offer insight into the behavior of the oxidation reaction when chlorine is not present in overwhelming excess, and allow the most appropriate form(s) of the rate expression to be determined. Variations in temperature should also be evaluated since the experimental data used in this study was limited to 20°C, with the mechanistic model allowing these temperature effects to be appropriately accounted for in a physically-based fashion. Effects of pH, and the presence of additional species (such as DOC) could also be considered, as well as different media types (sand, anthracite, garnet) and media grain sizes. The thickness of the MnO_x(s) coating, and thus the available surface area for adsorption, could have a substantial impact on the effective removal of Mn.

In contrast to the mechanistic model, the simple model ignores several key mechanisms, with the fitted rate constant essentially becoming a lumped parameter that accounts for these effects. While the mechanistic model avoids these simplifications, it nevertheless requires several additional parameters to be evaluated, and has a higher computational cost. Provided that its limitations are clearly understood, the simple model can therefore serve as a design tool, allowing useful insights into system performance. As a better understanding of the physical characteristics of the media coatings become available, and the rate expression is more comprehensively characterized, the mechanistic model could ultimately replace the simple model for design purposes.

Before using either model in a design application, the limitations of the models and current knowledge of the reaction mechanism should be well understood. Values determined in this study for k_r and $k_{r,1}$ are applicable to the source water and operating conditions used in generating the experimental data. Changes in source water quality may interfere with the adsorption and oxidation processes. At lower chlorine concentrations than those used in this study, the reaction mechanism may be best described as a second-order reaction which is dependent on chlorine, rather than a first-order reaction, which is not. Therefore in any design application, bench- or pilot-scale studies should be performed prior to using either model. These studies should be used to find the appropriate form of both the adsorption isotherm and the oxidation rate expression. Once the constants associated with these are available, the models can be used to predict performance in a full-scale contactor column.

5.0 Conclusions

Two models of manganese sorption and surface oxidation in a contactor column were applied to experimental data from a pilot-scale experiment. Both models fit the data well, with fitted k_r values on the order of 10^{-3} to 10^{-2} m^3 mol^{-1} s^{-1}. Differences in fitted k_r between the two models are attributed to differences in the available surface area for sorption of soluble Mn. An inverse relationship between fitted k_r and chlorine concentration was observed when chlorine was included in the reaction term, but the same relationship was not observed after removing chlorine, showing that at the chlorine concentrations studied, the rate of Mn oxidation depends only on the adsorbed concentration of manganese.

A sensitivity analysis showed that the Freundlich isotherm constants and reaction rate constant are most critical to predicting contactor column performance, while the effects of axial dispersion in the column are negligible.

The simple model should be useful for designing media contactor units for manganese removal, while the mechanistic model should be able to resolve differences (internal surface area and thickness) in the various types of oxide coating, and will allow a more fundamental and mechanistically-consistent evaluation of the appropriate form of the rate expression.

Works Cited

Bansal, R. C., & Goyal, M. (2005). *Activated Carbon Adsorption.* Boca Raton, Florida: Taylor & Francis.

Bouchard, R. (2005). *Evaluation of Manganese Removal at Aquarion Water Company (AWC) Surface Water Treatment Plants.* Master Thesis, University of Massachusetts, Department of Civil & Environmental Engineering, Amherst, MA.

Bryant, L. D., Hsu-Kim, H., Gantzer, P. A., & Little, J. C. (2011). Solving the problem at the source: Controlling Mn release at the sediment-water interface via hypolimnetic oxygenation. *Water Research , 45*, 6381-6392.

Buamah, R., Petrusevski, B., de Ridder, D., van de Wetering, T., & Shippers, J. C. (2009). Manganese removal in groundwater treatment: practice, problems and probable solutions. *Water Science & Technoogy , 9* (1), 89-98.

Cerrato, J. M., Knocke, W. R., Hochella, M. F Jr., Dietrich, A. M., Jones, A., & Cromer, T. F. (2011). Application of XPS and Solution Chemistry Analyses to Investigate Soluble Manganese Remoal by MnO_x(s)-coated Media. *Environmental Science and Technology, 45,* 10068-10074.

Coffey, B. M., Gallagher, D. L., & Knocke, W. R. (1993). Modeling soluble manganese removal by oxide-coated filter media. *Journal of Environmental Engineering , 119* (4), 679-694.

Davison, W. M., Pitts, B., & Stewart, P. S. (2010). Spatial and Temporal Patterns of Biocide Action against Staphylococcus epidermidis Biofilms. *Antimicrobial Agents and Chemotherapy , 54* (7), 2920-2927.

Delgado, J. (2007). Longitudinal and Transverse Dispersion in Porous Media. *Chemical Engineering Research and Design , 85*, 1245-1252.

Domenico, P. A., & Schwartz, F. W. (1998). *Physical and Chemical Hydrogeology* (2nd ed.). John Wiley & Sons.

Gantzer, P. A., Bryant, L. D., & Little, J. C. (2009). Controlling soluble iron and manganese in a water-supply reservoir using hypolimnetic oxygenation. *Water Research* (43), 1285-1294.

Gregory, D., & Carlson, K. H. (2003). Impact of Soluble Manganese Concentration on Oxidation Kinetics. *Journal AWWA , 95* (1), 98-108.

Homoncik, S. C., MacDonald, A. M., Heal, K. V., O Dochartaigh, B. E., & Ngwenya, B. T. (2010). Manganese Concentrations in Scottish groundwater. *Science of the Total Environment , 408*, 2467-2473.

Hua, G., & Reckhow, D. A. (2007). Comparison of disinfection byproduct formation from chlorine and alternative disinfectants. *Water Research , 41*, 1667-1678.

Knocke, W. R., Zuravnsky, L., Little, J. C., & Tobiason, J. E. (2010). Adsorptive contactors for removal of soluble manganese during drinking water treatment. *Journal AWWA , 102* (8), 64-75.

Kohl, P., & Medlar, S. *Occurence of Manganese in Drinking Water and Manganese Control.* Denver: AWWA Research Foundation and AWWA.

Merkle, P. B., Knocke, W. R., Gallagher, D. L., & Little, J. C. (1997). Dynamic model for soluble Mn2+ removal by oxide-coated filter media. *Journal of Environmental Engineering , 123* (7), 650-658.

Mouchet, P. (1992). From Conventional to Biological Removal of Iron and Manganese in France. *Journal AWWA , 84* (4), 158-167.

Nakanishi, H. (1967). Kinetics of continuous removal of manganese in a MnO2-coated sand bed. *Kogyo Kagaku Zasshi , 70* (4), 407.

Pham, M. (2010). *Two-stage Filtration to Control Manganese and DBPS at the Lantern Hill Water Treatment Plant*. Masters Thesis, University of Massachusetts, Department of Civil and Environmental Engineering, Amherst, MA.

Roberts, P. V., Cornel, P., & Summers, R. S. (1985). External Mass-transfer Rate in Fixed-bed Adsorption. *Journal of Environmental Engineering , 111* (6), 891-905.

Sly, L. I., Hodgkinson, M. C., & Arunpairojana, V. (1990). Deposition of Manganese in a Drinking Water System. *Applied and Environmental Microbiology , 56* (3), 628-639.

Subramaniam, A. (2010). *A pilot-scale evaluation of soluble manganese removal using pyrolucite media in a high-rate adsorptive contactor.* Masters Thesis, Virginia Polytechnic Institute and State University, Department of Civil and Environmental Engineering, Blacksburg, VA.

Tobiason, J. E., Knocke, W. R., Goodwill, J., Islam, A. A., Hargette, P., Bouchard, R., et al. (2007). *Characterization and Performance of Filter Media for Manganese Control.* AWWA Research Foundation, US Environmental Protection Agency. AWWARF.

Zuravnsky, L. (2006). *Development of soluble manganese sorptive contactors for enhancing potable water treatment practices.* Masters Thesis, Virginia Polytechnic Institute and State University, Department of Civil and Environmental Engineering, Blacksburg, VA.

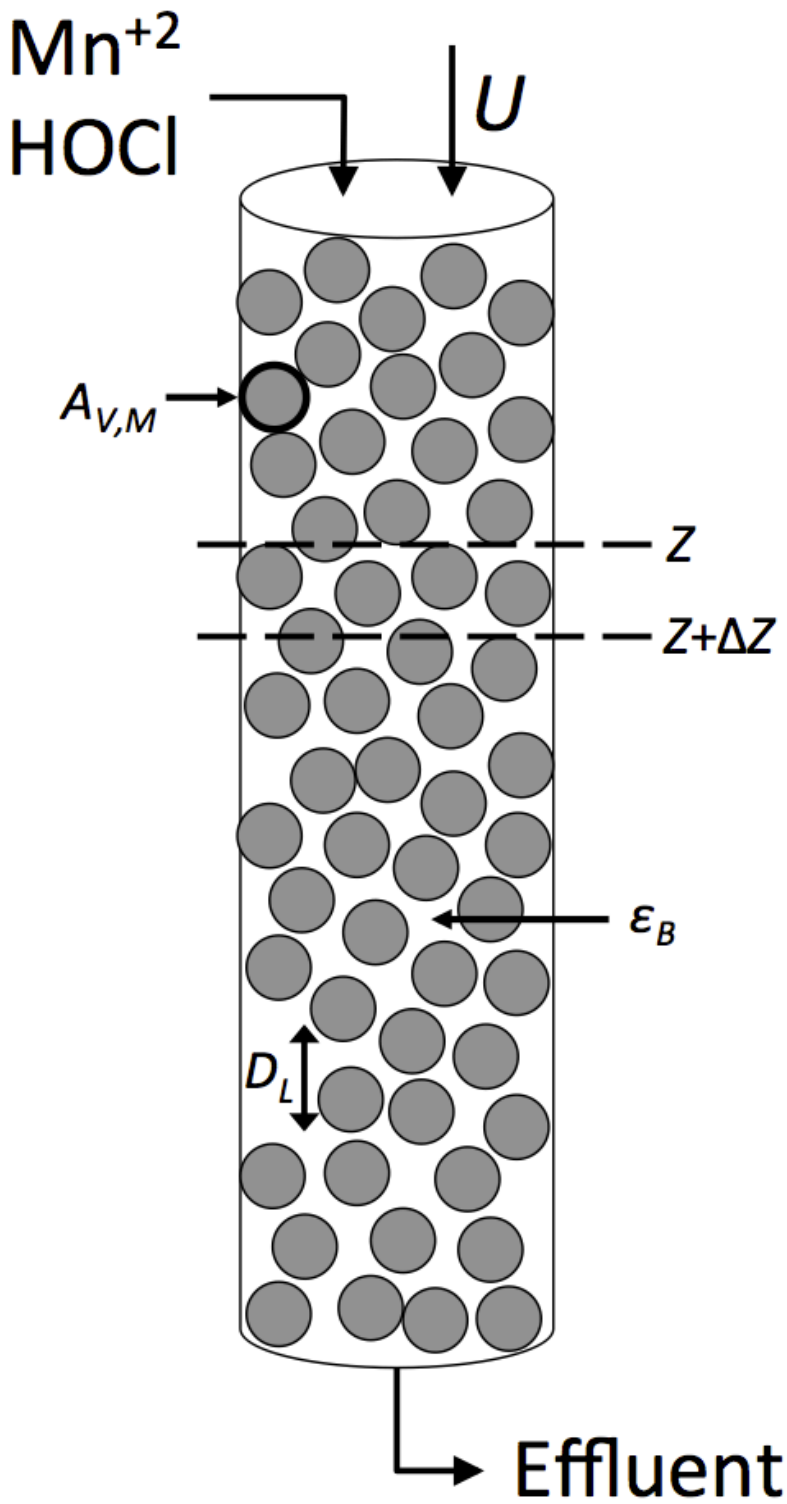

Figure 1. Schematic of a contactor column showing advection (U), axial dispersion (D_L), bed porosity (ε_B), and specific external surface area ($A_{V,M}$).

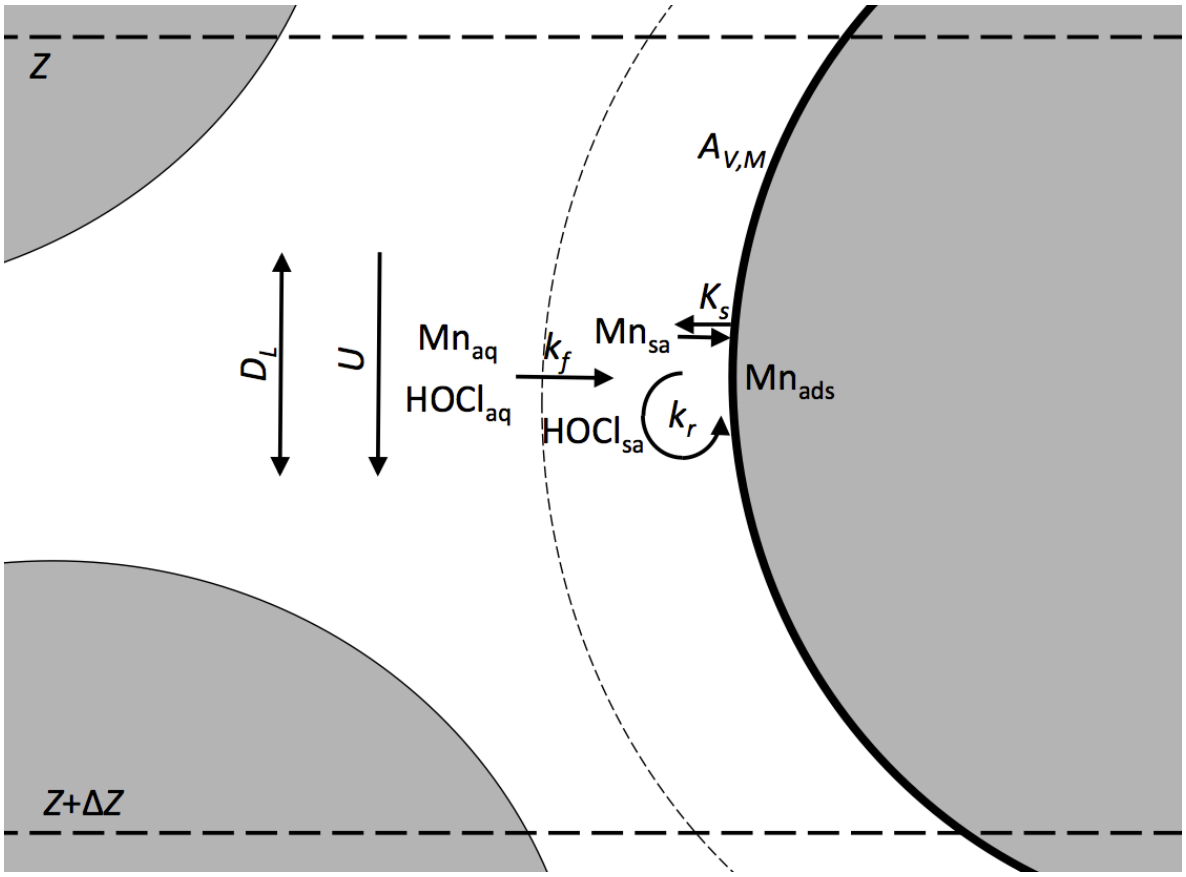

Figure 2. Schematic of a differential volume of media showing advection (U) and dispersion (D_L) in the bulk water, mass transfer (k_f) from the bulk water through the boundary layer, adsorptive equilibrium (K_s), chemical oxidation (k_r) of adsorbed Mn by chlorine, and specific external surface area ($A_{V,M}$).

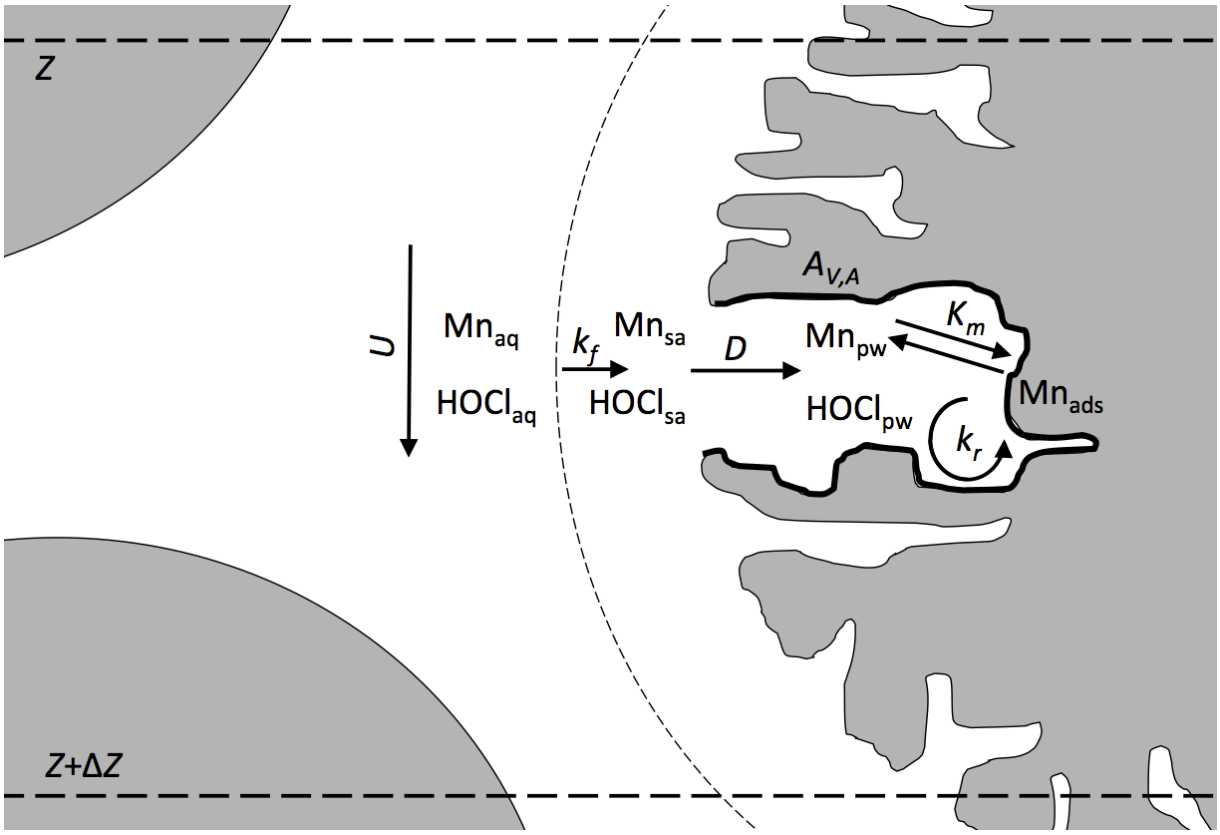

Figure 3. Schematic of a differential volume of media showing advection (U) in the bulk water, mass transfer (k_f) from the bulk water through the boundary layer, diffusion (D) from the boundary layer into the media pore water, adsorptive equilibrium (K_m), chemical oxidation (k_r) of adsorbed Mn by chlorine, and specific internal surface area ($A_{V,A}$).

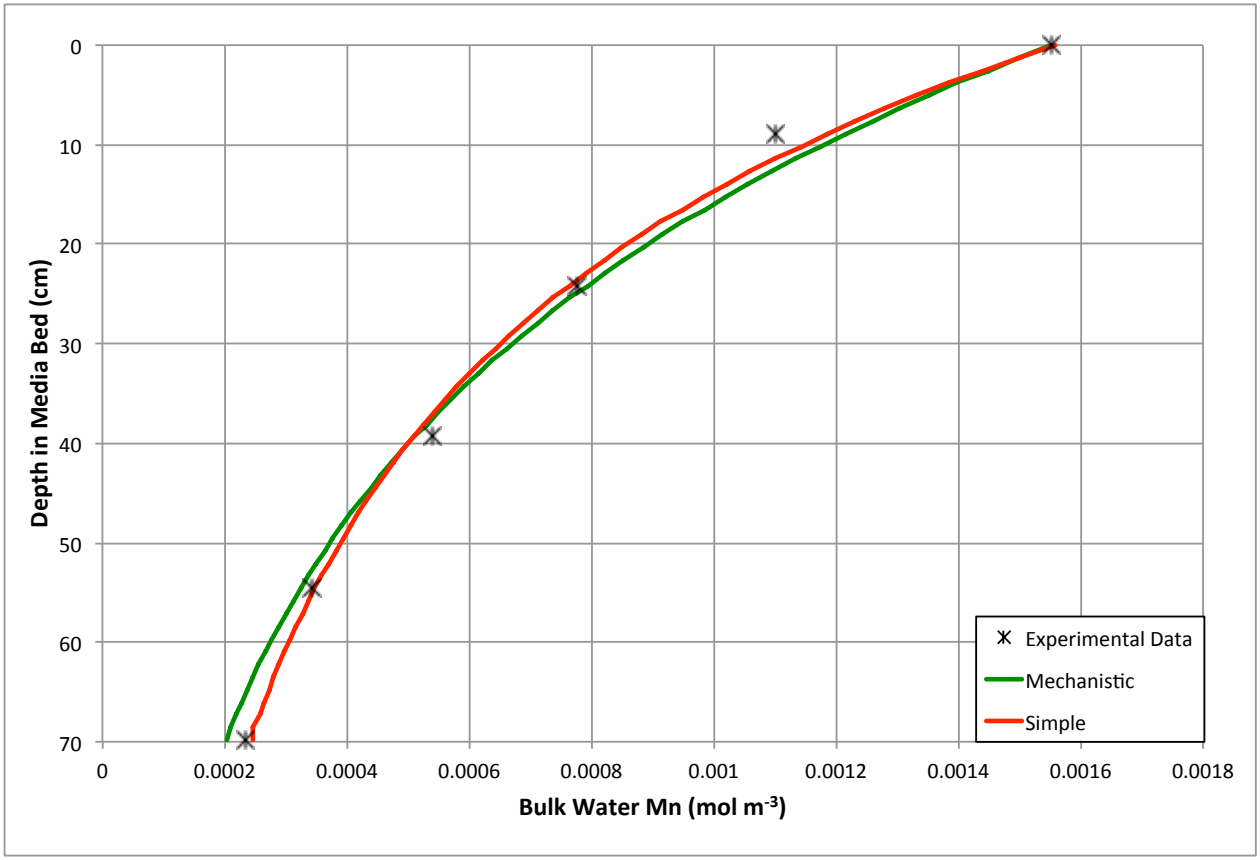

Figure 4. Bulk water manganese profiles from simple and mechanistic models fit to experimental profile data from run A6.

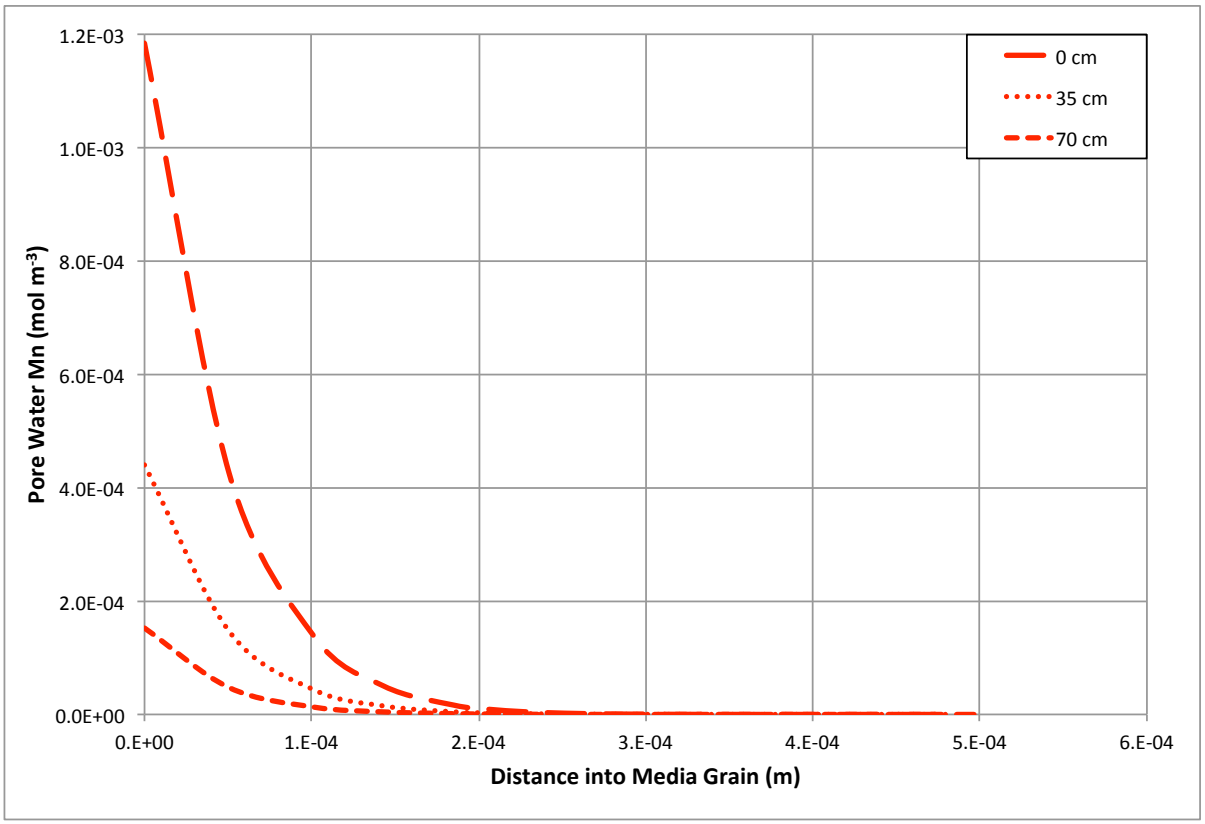

Figure 5. Mechanistic model predicted media pore water Mn profiles for media at depths of 0, 35, and 70 cm in the contactor column using conditions from run A6.

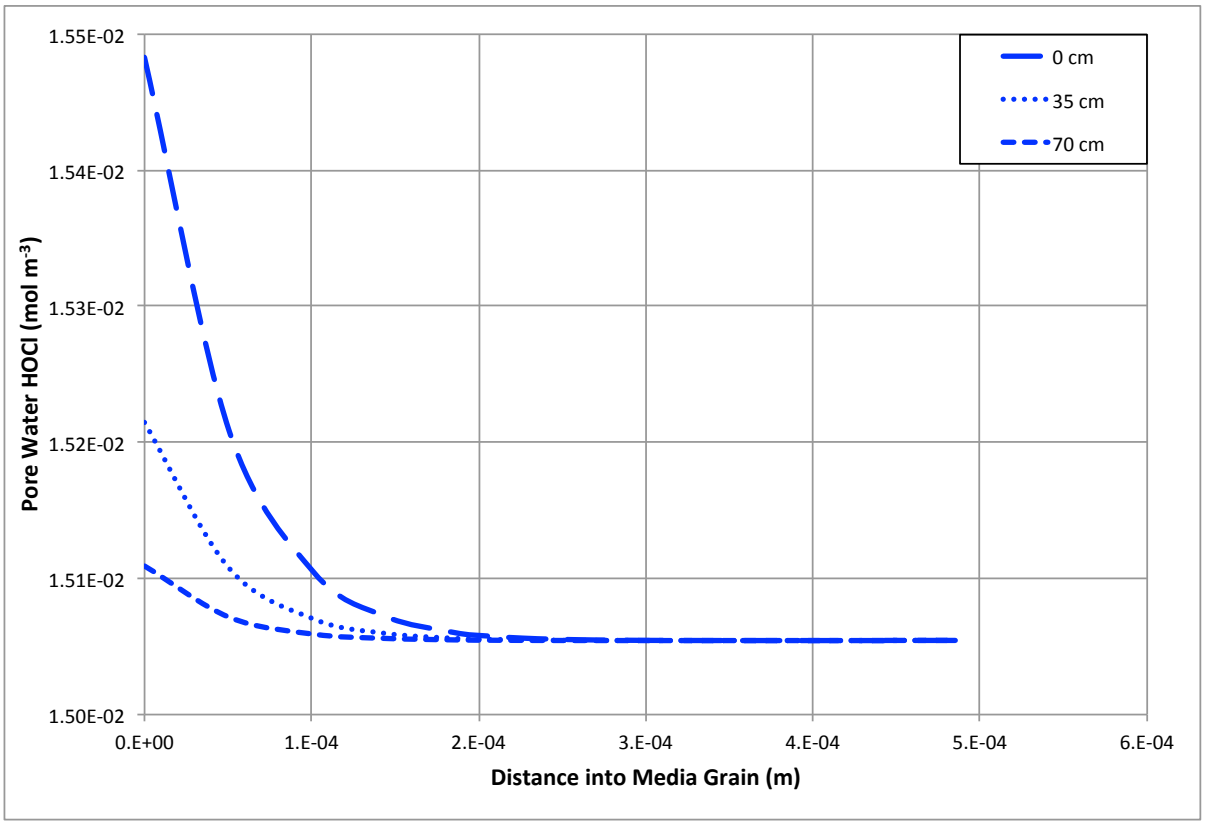

Figure 6. Mechanistic model predicted media pore water chlorine profiles for media at depths of 0, 35, and 70 cm in the contactor column using conditions from run A6.

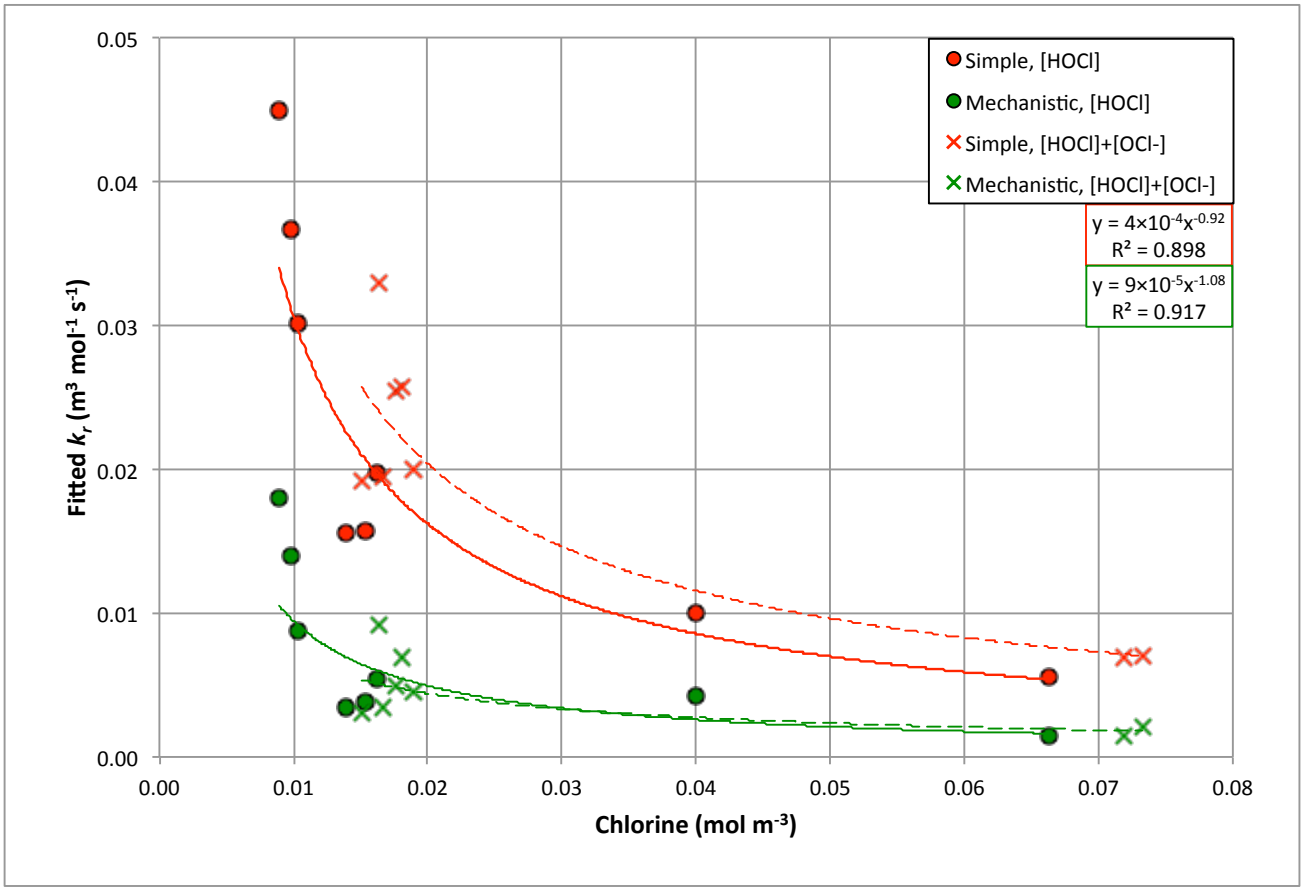

Figure 7. Oxidation rate constant (k_r) versus chlorine concentration, showing inverse relationship observed in both models using HOCl-only and HOCl+OCl$^-$ conditions. Boxed trend line equations correspond to solid trend lines on the chart.

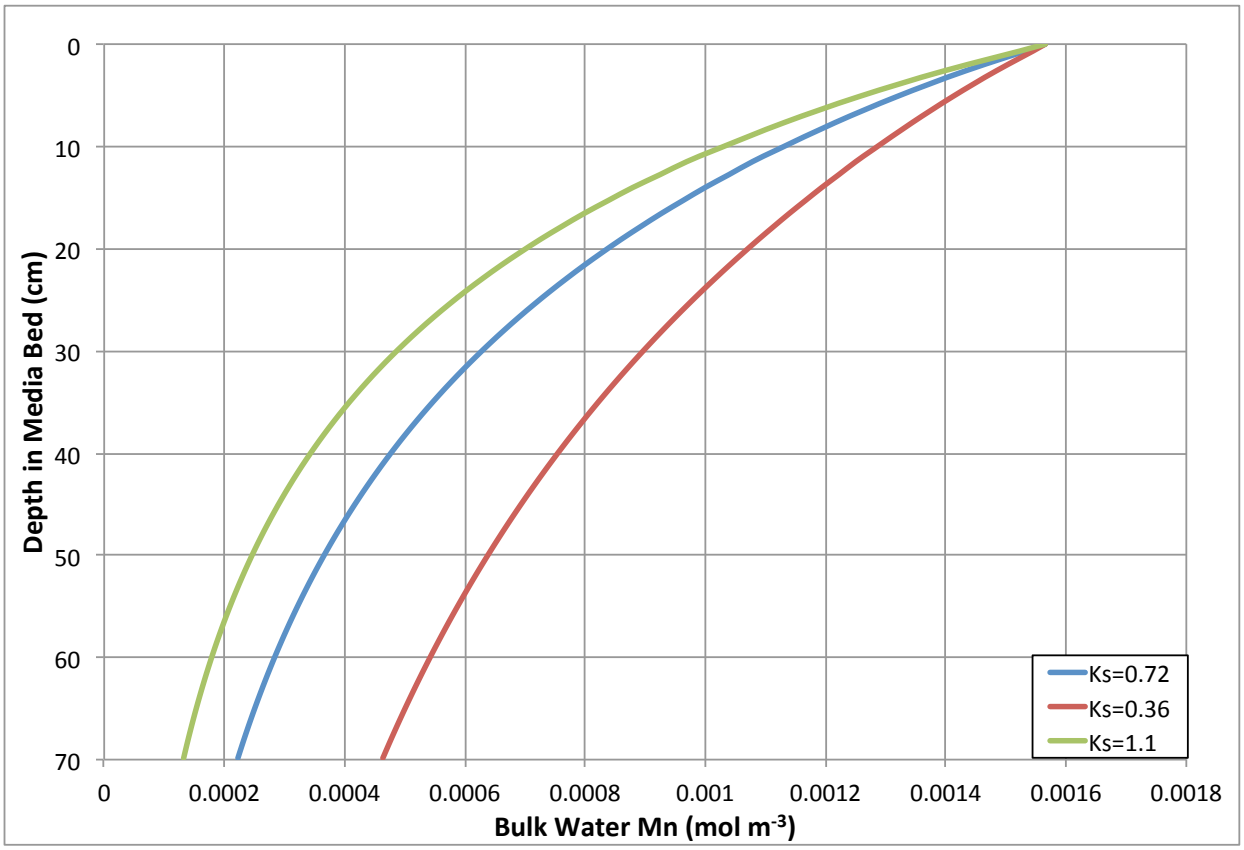

Figure 8. Effect of adjusting Freundlich K_s [units: (mol kg^{-1})(mol m^{-3})$^{-n}$] by ±50% on the simple model predicted bulk water manganese profile

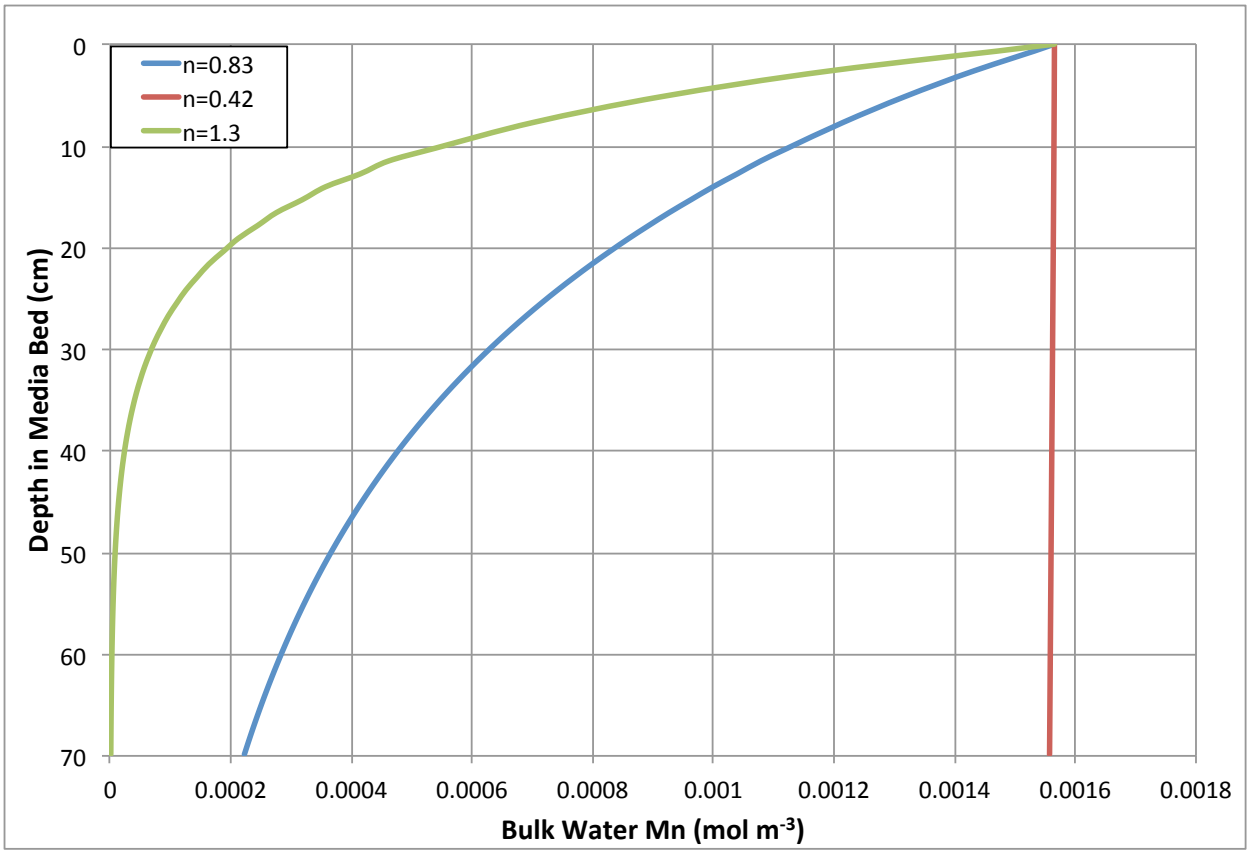

Figure 9. Effect of adjusting Freundlich *n* [dimensionless] by ±50% on the simple model predicted bulk water manganese profile

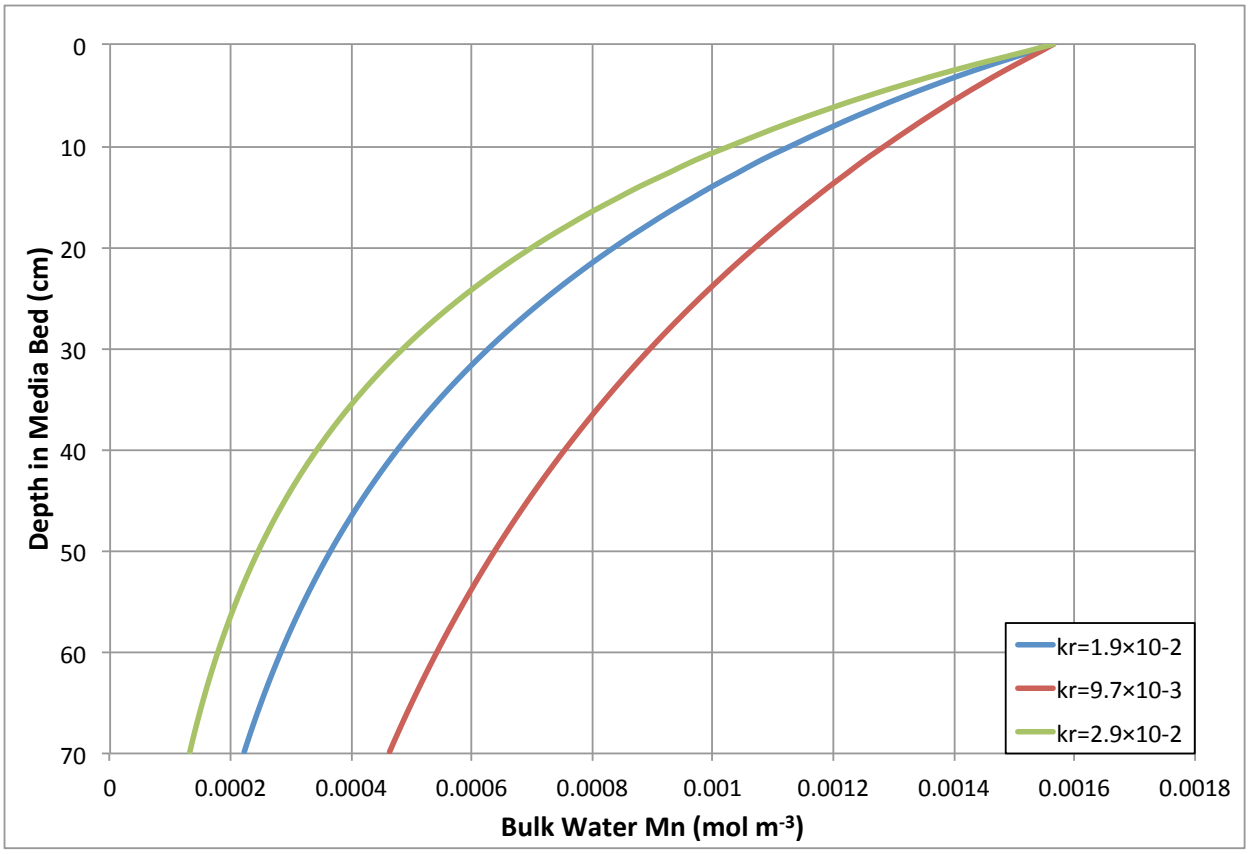

Figure 10. Effect of adjusting oxidation rate constant (k_r) [units: m^3 mol^{-1} s^{-1}] by ±50% on the simple model predicted bulk water manganese profile

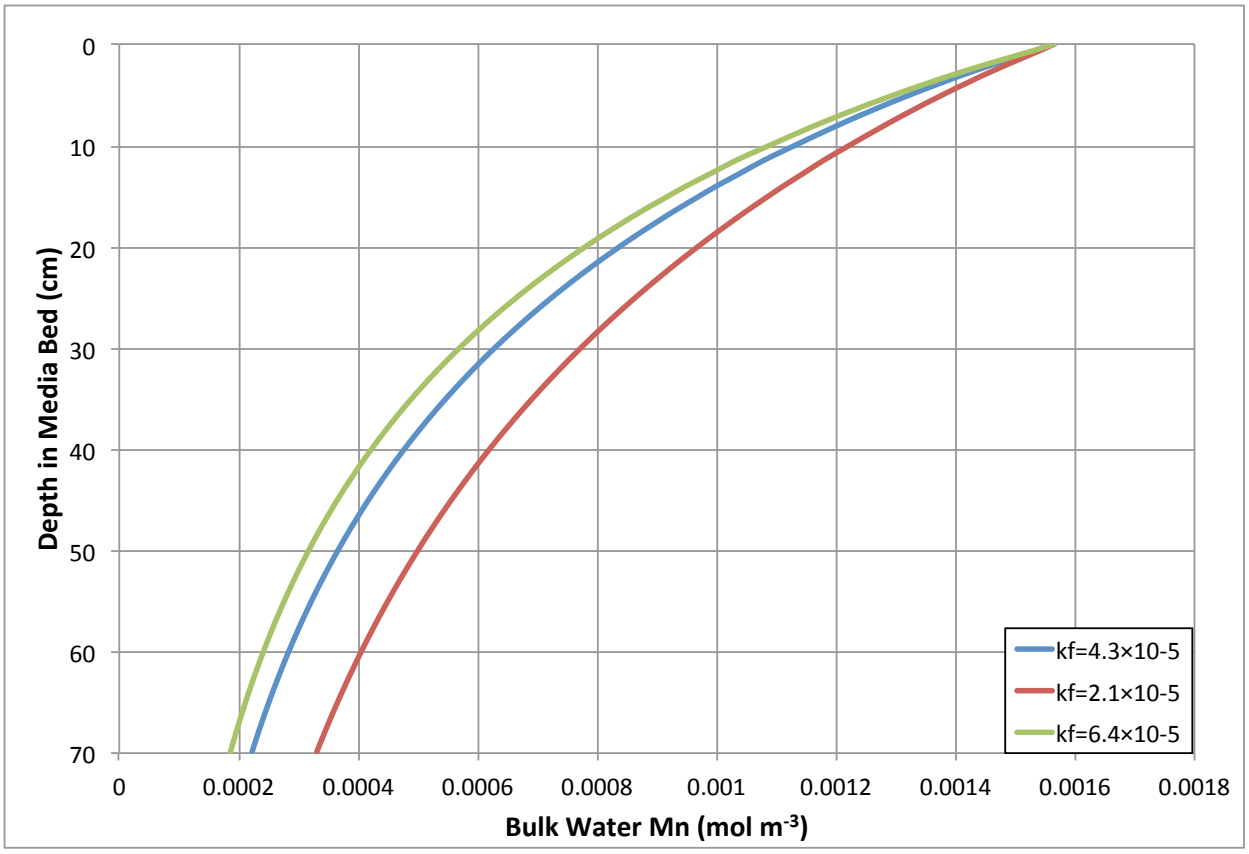

Figure 11. Effect of adjusting mass-transfer coefficient (k_f) [units: m s^{-1}] by ±50% on the simple model predicted bulk water manganese profile

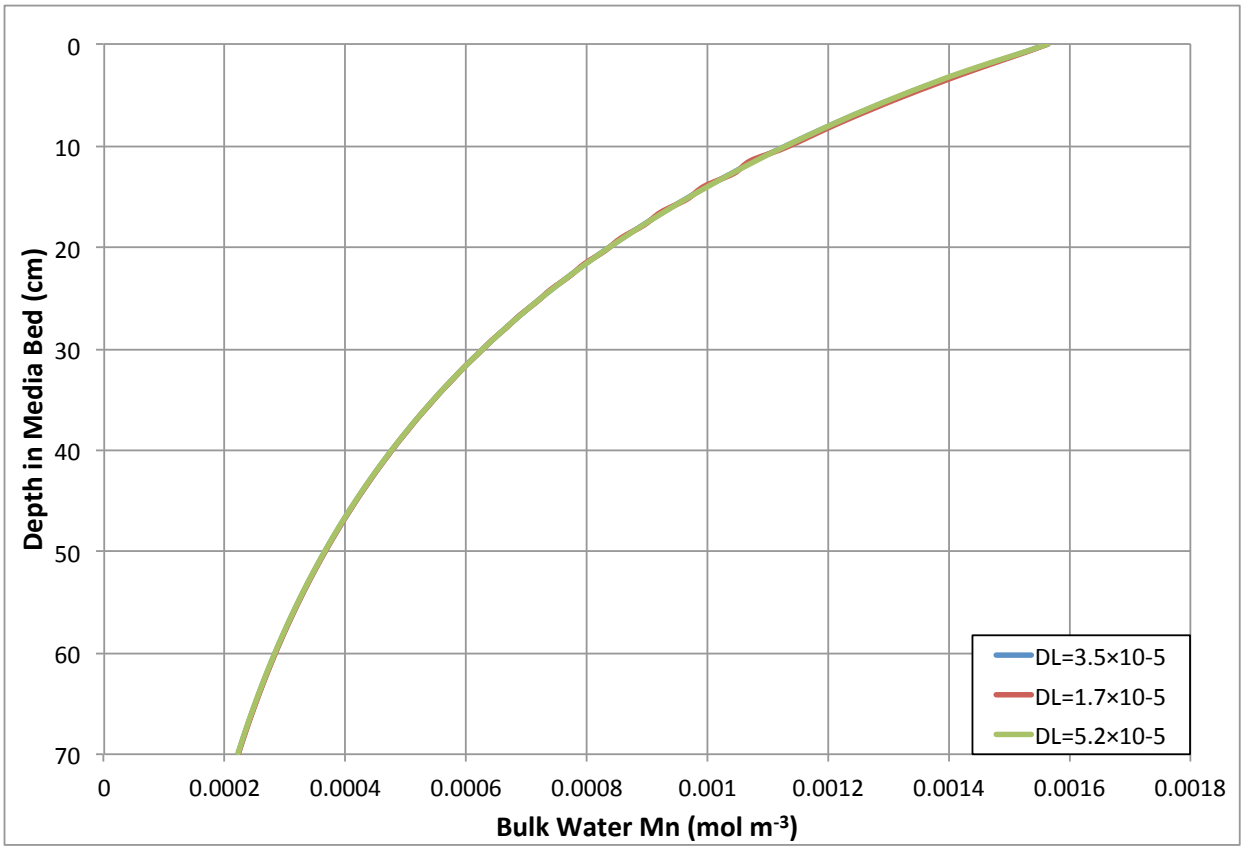

Figure 12. Effect of adjusting axial dispersion coefficient (D_L) [units: m^2 s^{-1}] by ±50% on the simple model predicted bulk water manganese profile

Table 1. Summary of fitted oxidation rate constant values

				Simple Model			Mechanistic Model	
Run	HLR ($m^3\ min^{-1}\ m^{-2}$)	pH	Total Chlorine ($mol\ m^{-3}$)	Fitted k_r [HOCl] ($m^3\ mol^{-1}\ s^{-1}$)	Fitted k_r [HOCl+OCl^-] ($m^3\ mol^{-1}\ s^{-1}$)	Fitted $k_{r,1}$ [Chlorine Removed] (s^{-1})	Fitted k_r [HOCl] ($m^3\ mol^{-1}\ s^{-1}$)	Fitted k_r [HOCl+OCl^-] ($m^3\ mol^{-1}\ s^{-1}$)
A1	0.98	7.5	7.3×10^{-2}	1.0×10^{-2}	7.1×10^{-3}	5.0×10^{-4}	4.3×10^{-3}	2.1×10^{-3}
A2	0.98	6.5	7.2×10^{-2}	5.6×10^{-3}	7.0×10^{-3}	4.9×10^{-4}	1.5×10^{-3}	1.5×10^{-3}
A3	0.98	6.5	1.8×10^{-2}	2.0×10^{-2}	2.6×10^{-2}	4.3×10^{-4}	5.4×10^{-3}	4.9×10^{-3}
A4	0.98	7.5	1.8×10^{-2}	3.7×10^{-2}	2.6×10^{-2}	4.4×10^{-4}	1.4×10^{-2}	6.9×10^{-3}
A5	0.82	7.5	1.6×10^{-2}	4.5×10^{-2}	3.3×10^{-2}	5.2×10^{-4}	1.8×10^{-2}	9.2×10^{-3}
A6	0.82	6.5	1.7×10^{-2}	1.6×10^{-2}	2.0×10^{-2}	3.1×10^{-4}	3.8×10^{-3}	3.5×10^{-3}
A7	0.65	6.5	1.5×10^{-2}	1.6×10^{-2}	1.2×10^{-2}	2.8×10^{-4}	3.5×10^{-3}	3.1×10^{-3}
A8	0.65	7.5	1.9×10^{-2}	3.0×10^{-2}	2.0×10^{-2}	3.6×10^{-4}	8.8×10^{-3}	4.5×10^{-3}
		Mean		2.2×10^{-2}	2.0×10^{-2}	4.2×10^{-4}	7.4×10^{-3}	4.5×10^{-3}
		Coefficient of Variation		0.61	0.46	0.22	0.78	0.57

Appendix A: Derivation of Simple Model Mass Balance Equations

This appendix outlines the derivation of mass balance equations used in the simple model. Variables are defined in the manuscript (Section 2.1 and equations 4-7).

Write a steady-state mass balance for manganese in a differential volume of contactor column, including terms for advection, dispersion, mass transfer and adsorptive equilibrium. A schematic of these processes is shown in Figure 2 of the manuscript.

$$\frac{\partial C_{1B}}{\partial t} = 0 = -U\frac{\partial C_{1B}}{\partial z} + D_L\frac{\partial^2 C_{1B}}{\partial z^2} - k_f A_{V,M}\left(\frac{1-\varepsilon_B}{\varepsilon_B}\right)\left(C_{1B} - \left[\frac{C_{1sa}}{K_s}\right]^n\right) \tag{A1}$$

Write a mass balance for Mn adsorbed to the media surface. Mass transfer, adsorptive equilibrium, and chemical oxidation determine the concentration as follows:

$$\frac{\partial C_{1sa}}{\partial t} = 0 = \frac{k_f A_{V,M}}{\rho_B}\left(1-\varepsilon_B\right)\left[C_{1B} - \left[\frac{C_{1sa}}{K_s}\right]^n\right] - k_r\varepsilon_B C_{1sa}C_{2B} \tag{A2}$$

Add $k_r\varepsilon_B C_{1sa}C_{2B}$ to both sides of equation A2:

$$k_r\varepsilon_B C_{1sa}C_{2B} = \frac{k_f A_{V,M}}{\rho_B}\left(1-\varepsilon_B\right)\left[C_{1B} - \left[\frac{C_{1sa}}{K_s}\right]^n\right] \tag{A3}$$

Multiply both sides by ρ_B/ε_B:

$$k_r\rho_B C_{1sa}C_{2B} = k_f A_{V,M}\left(\frac{1-\varepsilon_B}{\varepsilon_B}\right)\left[C_{1B} - \left[\frac{C_{1sa}}{K_s}\right]^n\right] \tag{A4}$$

Substitute equation A4 into equation A1 to obtain the bulk water Mn balance with terms for advection, dispersion, and oxidation:

$$\frac{\partial C_{1B}}{\partial t} = 0 = -U\frac{\partial C_{1B}}{\partial z} + D_L\frac{\partial^2 C_{1B}}{\partial z^2} - k_r\rho_B C_{1sa}C_{2B} \tag{A5}$$

Write a mass balance for chlorine with terms for advection, dispersion and oxidation. Note that after substituting equation A4 into equation A1, the Mn and chlorine mass balances have identical reaction terms.

$$\frac{\partial C_{2B}}{\partial t} = 0 = -U\frac{\partial C_{2B}}{\partial z} + D_L\frac{\partial^2 C_{2B}}{\partial z^2} - k_r\rho_B C_{1sa}C_{2B} \quad \text{(A6)}$$

After an inverse relationship between fitted k_r and chlorine concentration was observed, chlorine was removed from the reaction term. Equations A5 and A6 then become:

$$\frac{\partial C_{1B}}{\partial t} = 0 = -U\frac{\partial C_{1B}}{\partial z} + D_L\frac{\partial^2 C_{1B}}{\partial z^2} - k_{r,1}\rho_B C_{1sa} \quad \text{(A7)}$$

$$\frac{\partial C_{2B}}{\partial t} = 0 = -U\frac{\partial C_{2B}}{\partial z} + D_L\frac{\partial^2 C_{2B}}{\partial z^2} - k_{r,1}\rho_B C_{1sa} \quad \text{(A8)}$$

Appendix B: Derivation of Mechanistic Model Mass Balance Equations

This appendix outlines the derivation of the mass balance equations used in the mechanistic model. Variables are defined, with appropriate units, at the end of this appendix.

Bulk Water Mn Balance

Write a mass balance for a differential volume of contactor column, including terms for advection, dispersion, and mass transfer. A schematic of the processes involved is shown in Figure 3 of the manuscript.

$$\frac{\partial C_{1B}}{\partial t} = -U\frac{\partial C_{1B}}{\partial z} + D_L\frac{\partial^2 C_{1B}}{\partial z^2} - k_f A_{V,M}\left(\frac{1-\varepsilon_B}{\varepsilon_B}\right)\left(C_{1B} - C_{1sa}\right) \quad \text{(B1)}$$

Assume that the contactor is at steady state and that dispersion is negligible:

$$\frac{\partial C_{1B}}{\partial t} = 0 = -U\frac{\partial C_{1B}}{\partial z} - k_f A_{V,M}\left(\frac{1-\varepsilon_B}{\varepsilon_B}\right)\left(C_{1B} - C_{1sa}\right) \quad \text{Steady-state Equation (B2)}$$

Bulk Water Chlorine Balance

Write a mass balance for a differential volume of contactor column, including terms for advection, dispersion, and mass transfer:

$$\frac{\partial C_{2B}}{\partial t} = -U\frac{\partial C_{2B}}{\partial z} + D_L\frac{\partial^2 C_{2B}}{\partial z^2} - k_f A_{V,M}\left(\frac{1-\varepsilon_B}{\varepsilon_B}\right)\left(C_{2B} - C_{2sa}\right) \quad \text{(B3)}$$

Assume that the contactor is at steady state and that dispersion is negligible:

$$\frac{\partial C_{2B}}{\partial t} = 0 = -U\frac{\partial C_{2B}}{\partial z} - k_f A_{V,M}\left(\frac{1-\varepsilon_B}{\varepsilon_B}\right)\left(C_{2B} - C_{2sa}\right) \quad \text{Steady-state Equation (B4)}$$

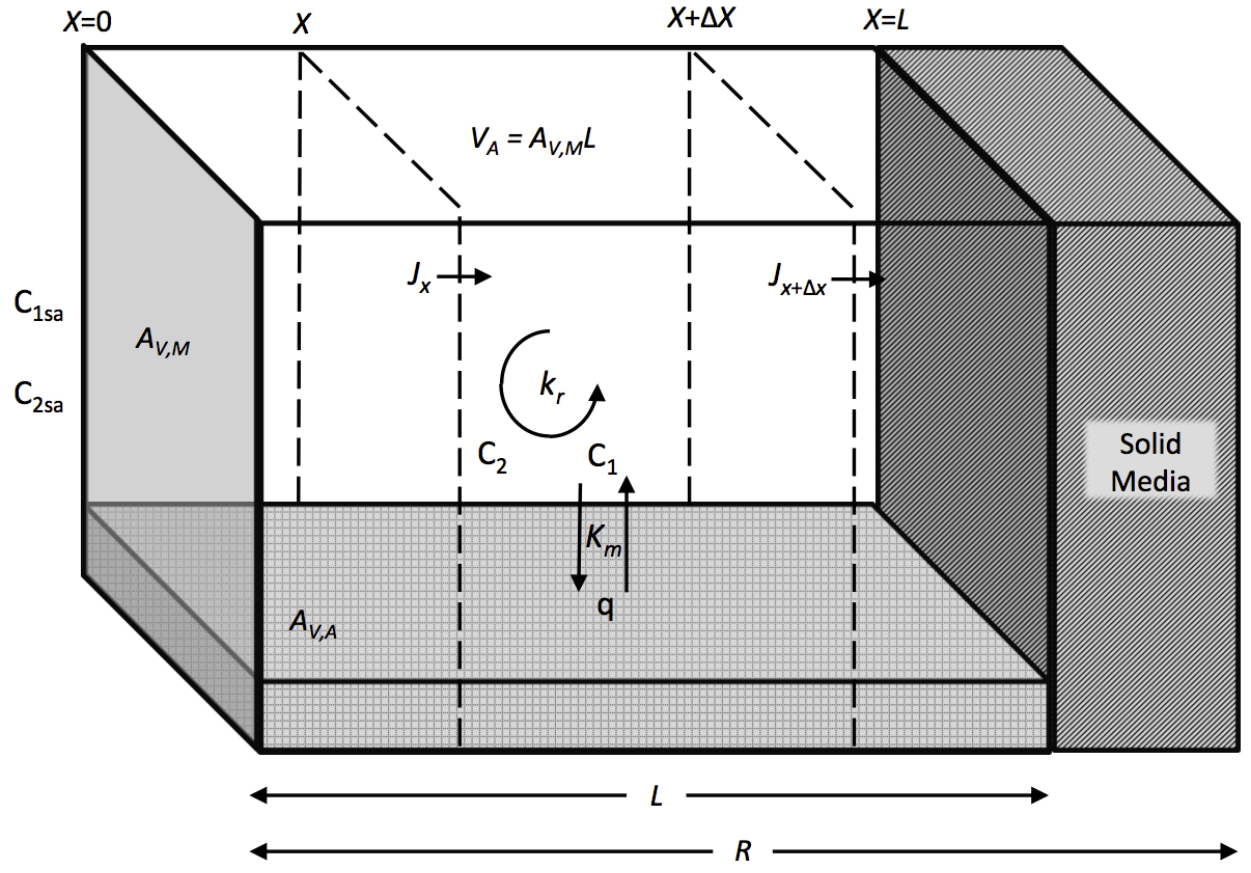

Figure B 1. Simplified schematic of media pore, showing diffusive flux (*J*), adsorption (K_m), reaction (k_r), and relevant physical characteristics.

Media Pore Water Mn Balance

Accumulation of manganese in the media pore water is expressed as:

Accumulation in media pore water + Accumulation adsorbed = Diffusive flux – Reaction

Converting into mathematical terms:

$$\Delta C_1 \varepsilon_A \Delta x A_{V,M} V_g + \Delta q \frac{A_p}{V_A} \Delta x A_{V,M} V_g = \Delta J_1 \Delta t A_{V,M} V_g - k_r q \frac{A_p}{V_A} \varepsilon_A A_{V,M} V_g C_2 \Delta t \Delta x \qquad \text{(B5)}$$

Note: In this case, $A_{V,M}$ has units of $m^2_{active\ grain}\ m^{-3}_{grain}$. Since the external surface area of the entire grain is identical to the external surface area of the active grain, the value of $A_{V,M}$ in units of $m^2_{grain}\ m^{-3}_{grain}$ and $m^2_{active\ grain}\ m^{-3}_{grain}$ is identical.

Divide both sides by $A_{V,M}V_g\varepsilon_A\Delta t\Delta x$ which yields:

$$\frac{\Delta C_1}{\Delta t}+\frac{\Delta q}{\Delta t}\left(\frac{A_p}{V_A\varepsilon_A}\right)=\frac{1}{\varepsilon_A}\frac{\Delta J_1}{\Delta x}-k_r q\frac{A_p}{V_A}C_2 \tag{B6}$$

Allowing Δt and Δx to tend to zero:

$$\frac{\partial C_1}{\partial t}+\frac{\partial q}{\partial t}\left(\frac{A_p}{V_A\varepsilon_A}\right)=\frac{1}{\varepsilon_A}\frac{\partial J_1}{\partial x}-k_r q\frac{A_p}{V_A}C_2 \tag{B7}$$

By definition:

$$q=K_m C_1^n \quad \text{and} \quad J_1=-D_1\frac{\partial C_1}{\partial x} \tag{B8, B9}$$

Therefore:

$$\frac{\partial q}{\partial t}=\frac{\partial K_m C_1^n}{\partial t}=K_m\frac{\partial C_1^n}{\partial t} \quad \text{and} \quad \frac{\partial J_1}{\partial x}=\frac{\partial}{\partial x}\left(-D_1\frac{\partial C_1}{\partial x}\right)=-D_1\frac{\partial^2 C_1}{\partial x^2} \tag{B10, B11}$$

Also:

$$A_{V,A}=\frac{A_p}{V_A} \tag{B12}$$

Substitute equations B10, B11, and B12 into equation B7**:**

$$\frac{\partial C_1}{\partial t}+\left(\frac{A_{V,A}K_m}{\varepsilon_A}\right)\frac{\partial C_1^n}{\partial t}=-\frac{D_1}{\varepsilon_A}\frac{\partial^2 C_1}{\partial x^2}-k_r A_{V,A}K_m C_1^n C_2 \tag{B13}$$

Using the chain rule:

$$\frac{\partial C_1^n}{\partial t}=\left(nC_1^{n-1}\right)\frac{\partial C_1}{\partial t} \tag{B14}$$

Substitute this expression into equation B13

$$\frac{\partial C_1}{\partial t}+\left(\frac{A_{V,A}K_m n C_1^{n-1}}{\varepsilon_A}\right)\frac{\partial C_1}{\partial t}=-\frac{D_1}{\varepsilon_A}\frac{\partial^2 C_1}{\partial x^2}-k_r A_{V,A}K_m C_1^n C_2 \qquad \text{(B15)}$$

Factor the left side of equation B15:

$$\frac{\partial C_1}{\partial t}\left(1+\frac{A_{V,A}K_m n C_1^{n-1}}{\varepsilon_A}\right)=-\frac{D_1}{\varepsilon_A}\frac{\partial^2 C_1}{\partial x^2}-k_r A_{V,A}K_m C_1^n C_2 \qquad \text{(B16)}$$

Now define a retardation factor, *R* as:

$$R=\left(1+\frac{A_{V,A}K_m n C_1^{n-1}}{\varepsilon_A}\right) \qquad \text{(B17)}$$

Substitute equation B17 into equation B16**:**

$$\frac{\partial C_1}{\partial t}R=-\frac{D_1}{\varepsilon_A}\frac{\partial^2 C_1}{\partial x^2}-k_r A_{V,A}K_m C_1^n C_2 \qquad \text{(B18)}$$

At steady state**:**

$$\frac{\partial C_1}{\partial t}R=0=-\frac{D_1}{\varepsilon_A}\frac{\partial^2 C_1}{\partial x^2}-k_r A_{V,A}K_m C_1^n C_2 \qquad \text{Steady-state Equation (B19)}$$

Media Pore Water Chlorine Balance

Write a mass balance for chlorine in the media pore water:

Accumulation in media pore water = Diffusive flux – Reaction

Expressing this in mathematical terms:

$$\Delta C_2 \varepsilon_A \Delta x A_{V,M} V_g = \Delta J_2 \Delta t A_{V,M} V_g - k_r q \frac{A_p}{V_A}\varepsilon_A A_{V,M} V_g C_2 \Delta t \Delta x \qquad \text{(B20)}$$

Note: In this case, $A_{v,M}$ has units of $m^2_{\text{active grain}}\ m^{-3}_{\text{grain}}$. Since the external surface area of the entire grain is identical to the external surface area of the active grain, the value of $A_{v,M}$ in units of $m^2_{\text{grain}}\ m^{-3}_{\text{grain}}$ and $m^2_{\text{active grain}}\ m^{-3}_{\text{grain}}$ is identical.

Divide both sides by $A_{V,M}V_g\varepsilon_A\Delta t\Delta x$ which yields:

$$\frac{\Delta C_2}{\Delta t} = \frac{1}{\varepsilon_A}\frac{\Delta J_2}{\Delta x} - k_r q \frac{A_p}{V_A} C_2 \tag{B21}$$

Allowing Δt and Δx to tend to zero:

$$\frac{\partial C_2}{\partial t} = \frac{1}{\varepsilon_A}\frac{\partial J_2}{\partial x} - k_r q \frac{A_p}{V_A} C_2 \tag{B22}$$

By definition:

$$J_2 = -D_2 \frac{\partial C_2}{\partial x} \tag{B23}$$

So:

$$\frac{\partial J_2}{\partial x} = \frac{\partial}{\partial x}\left(-D_2 \frac{\partial C_2}{\partial x}\right) = -D_2 \frac{\partial^2 C_2}{\partial x^2} \tag{B24}$$

Also:

$$A_{V,A} = \frac{A_p}{V_A} \tag{B25}$$

Substituting equations B24 and B25 into equation B22:

$$\frac{\partial C_2}{\partial t} = -\frac{D_2}{\varepsilon_A}\frac{\partial^2 C_2}{\partial x^2} - k_r A_{V,A} K_m C_1^n C_2 \tag{B26}$$

At steady state:

$$\frac{\partial C_2}{\partial t} = 0 = -\frac{D_2}{\varepsilon_A}\frac{\partial^2 C_2}{\partial x^2} - k_r A_{V,A} K_m C_1^n C_2 \qquad \text{Steady-state Equation} \tag{B27}$$

Additional Relationships

$$\varepsilon_B = \frac{V_{voids}}{V_{bed}} \tag{B28}$$

$$V_{media} = V_{bed}\left(1-\varepsilon_B\right) \tag{B29}$$

$$A_{media} = V_{media} A_{V,M} \tag{B30}$$

$$A_{grain} = V_g A_{V,M} \tag{B31}$$

Note: The value of A_{media} with units of m^2_{grain} is equivalent to A_{media} with units of $m^2_{active\ grain}$ because the external surface area of the media grain is equal to the external surface area of the active grain

$$V_A = A_{grain} L \tag{B32}$$

(A_{grain} units: $m^2_{active\ grain}$)

$$\varepsilon_A = \frac{V_{pore}}{V_A} \tag{B33}$$

$$L = \frac{V_{pore}}{A_{pore}} \tag{B34}$$

Note: In this equation, V_{pore} has units of $m^3_{active\ grain}$. V_{pore} would be measured as m^3_{water}, but since it measures internal media pore space, V_{pore} in m^3_{water} is equivalent to V_{pore} in $m^3_{active\ grain}$.

Variable	Units	Description
A_{grain}	m^2_{grain}	Surface area of individual media grain
A_{media}	m^2_{media}	Surface area of media in filter bed
A_p	$m^2_{active\ grain}$	Internal active pore surface area of grain
A_{pore}	$m^2_{active\ grain}$	Area of active grain pore opening
$A_{V,M}$	$m^2_{media}\ m^{-3}_{media}$	Specific external surface area of media
$A_{V,A}$	$m^2_{active\ grain}\ m^{-3}_{active\ grain}$	Specific internal surface area of active grain
C_1	mol Mn m^{-3}_{water}	Mn concentration in media grain pore water
C_{1B}	mol Mn m^{-3}_{water}	Bulk water Mn concentration
C_{1sa}	mol Mn m^{-3}_{water}	Mn concentration at media particle surface
C_2	mol HOCl m^{-3}_{water}	HOCl concentration in media grain pore water
C_{2B}	mol HOCl m^{-3}_{water}	Bulk water HOCl concentration
C_{2sa}	mol HOCl m^{-3}_{water}	HOCl concentration at media particle surface
D_1	$m^3_{water}\ m^{-1}_{active\ grain}\ s^{-1}$	Mn diffusion coefficient
D_2	$m^3_{water}\ m^{-1}_{active\ grain}\ s^{-1}$	HOCl diffusion coefficient
D_L	$m^2\ s^{-1}$	Dispersion coefficient
ε_A	$m^3_{water}\ m^{-3}_{active\ grain}$	Porosity of active grain
ε_B	$m^3_{water}\ m^{-3}_{bed}$	Fractional pore volume of filter bed
J_1	mol Mn $m^{-2}_{active\ grain}\ s^{-1}$	Mn diffusive flux; based on cross sectional area of grain
J_2	mol HOCl $m^{-2}_{active\ grain}\ s^{-1}$	HOCl diffusive flux; based on cross sectional area of grain

K_m	$(\text{mol m}^{-2}_{\text{active grain}})/(\text{mol m}^{-3}_{\text{water}})^n$	Isotherm constant
k_f	m s^{-1}	Mass transfer coefficient
k_r	$\text{m}^3_{\text{active grain}}\ \text{mol}^{-1}\ \text{s}^{-1}$	Oxidation rate constant
L	$\text{m}_{\text{active grain}}$	Depth into active grain from surface
n	dimensionless	Isotherm constant
ρ	$\text{kg}_{\text{grain}}\ \text{m}^{-3}_{\text{grain}}$	Density of media grain
q	$\text{mol Mn m}^{-2}_{\text{active grain}}$	Sorbed phase Mn
t	s	Time
U	m s^{-1}	Colum pore water velocity
V_A	$\text{m}^3_{\text{active grain}}$	Active volume of grain
V_{bed}	m^3_{bed}	Volume of filter bed
V_g	$\text{m}^3_{\text{grain}}$	Volume of individual grain
V_{media}	$\text{m}^3_{\text{media}}$	Volume of media in filter bed
V_{pore}	$\text{m}^3_{\text{water}}$	Media pore volume of active grain
V_{voids}	$\text{m}^3_{\text{water}}$	Volume of voids in filter bed
x	$\text{m}_{\text{active grain}}$	Depth into media grain
z	m	Depth in filter bed
$1-\varepsilon_B$	$\text{m}^3_{\text{media}}\ \text{m}^{-3}_{\text{bed}}$	Fractional media volume of filter bed

Note: “Active grain” refers to the porous $MnO_x(s)$ coated portion of the media grains, which are active in the sense that they provide surface area for the Mn to be adsorbed and oxidized by chlorine. Any solid portion of the media grain underlying the porous $MnO_x(s)$ coating is not considered active. The terms “grain” and “media” refer to the entire grain of media, including the active and non-active portions.